Received: 9 December 2025 | Accepted: 23 March 2026

DOI: 10.1002/mawe.70124

RESEARCH ARTICLE

WILEY VCH

Microstructural evolution of V-Ti-B based high-temperature alloys during surface conditioning by means of laser beam melting

Entwicklung der Gefüge von V-Ti-B-Hochtemperatur-Legierungen während der Oberflächenmodifikation mittels selektivem Laserstrahlschmelzen

M. Carrion Saldaña[1] | W. Yang[2] | G. Hasemann[3] | H.-J. Christ[1] | R. Schwaiger[2, 4] | M. Krüger[3] | B. Gorr[5] | A. von Hehl[1]

[1]University of Siegen, Institute for Materials Engineering, Paul-Bonatz-Str. 9-11, 57076 Siegen, Germany

[2]Forschungszentrum Jülich GmbH, Institute of Energy and Climate Research, Structure and Function of Materials (IEK-2), Wilhelm-Johnen-Straße, 52428 Jülich, Germany

[3]Otto-von-Guericke Universität Magdeburg, Institute of Materials and Joining Technology, Universitätsplatz 2, 39106 Magdeburg, Germany

[4]RWTH Aachen University, Chair of Energy Engineering Materials, Faculty 5, Tempelgraben 55, 52056 Aachen, Germany

[5]Karlsruhe Institute of Technology (KIT), Institute for Applied Materials – Applied Materials Physics (Iadditive manufacturing (AM)-additive manufacturing (AM)P), Hermann-von-Helmholtz-Platz 1, 76344 Eggenstein-Leopoldshafen, Germany

Correspondence
M. Carrion Saldaña, University of Siegen, Institute for Materials Engineering, Paul-Bonatz-Str. 9-11, 57076 Siegen, Germany.
Email: mustafa.carrionsaldana@uni-siegen.de

Abstract

Respecting the potential of additive manufacturing (AM) technologies to enhance material performance, this article presents the first results of an investigation on the use of laser beam melting (LBM) on V-Ti-B alloys. Latter possess a high melting point and low density which are required for high-temperature structural applications. The research objective is to demonstrate the feasibility of the laser beam melting (LBM) technique to create graded microstructures and therefore to modify alloy properties throughout the specimen. Two values of the laser beam power were applied. The microstructural evolution of alloys with varying titanium and boron concentrations was examined by conducting scanning electron microscopy (SEM) and energy dispersive x ray spectroscopy (EDS) analyses throughout the entire process. Hardness measurements performed in the core of the samples as well as on the laser beam treated surfaces demonstrated that the surface conditioning of the V-Ti-B alloys result in higher hardness values, with increases ranging from 70 HV 10 (approx. 5 %; alloy V–28Ti–40B; 120 W) to 500 HV 10 (approx. 33%; alloy V–28Ti–40B; 180 W) compared to the intrinsic hardness of alloys in the arc–melted conditions. The experimental results clearly show that the fine microstructure is more favorable for the laser beam melting (LBM) application.

KEYWORDS
V-Ti-B alloys, surface conditioning, laser beam melting, additive manufacturing, refractory metals

SCHLÜSSELWÖRTER
V-Ti-B-Legierungen, Oberflächenstrukturierung, LPBF, Additive Fertigung, Refraktärmetalle

1 | INTRODUCTION

Novel high-temperature structural materials should exhibit a balanced combination of essential properties such as high-temperature strength, creep and oxidation resistance. Besides, the alloy density plays a significant role in applications where extra weight is directly related to additional costs, e.g. in aircraft applications. The use of vanadium as a base metal in alloys offers the advantage of a notably low density (ρ = 6.11 g/cm^3) compared to conventional Ni-based superalloys or high-temperature materials based on molybdenum and niobium [1]. Alloys that consist mostly of vanadium solid solution (V_{ss}), for example, V–(3.9…4.9)Cr–(4.2…5.3)Ti have been investigated as potential structural materials for fusion reactors [2]. In general, the potential use of V–based materials is restricted to inert atmospheres because pure vanadium or vanadium with minor additions exhibit inadequate resistance to oxidation under ambient atmospheric conditions. However, experimental investigations have demonstrated that additions of elements such as titanium, chromium, aluminum, silicon, and boron can effectively improve the oxidation resistance at elevated temperatures within the range of 800 °C to 900 °C [3,4].

The simultaneous additions of silicon and boron to vanadium result in the development of a three-phase microstructure comprising vanadium solid solution and intermetallic phases, namely V_3Si and V_5SiB_2. Preliminary studies conducted on the V-Si-B system recognized the V_5SiB_2 phase as a phase exhibiting notable resistance to oxidation [5].

Microhardness measurements indicate that the presence of intermetallic phases substantially impacts the hardness of the V_{ss}–V_3Si–V_5SiB_2 multi-phase alloy [1]. The hardness of alloys including intermetallic phases is approximately twofold compared to the single-phase V_{ss} (700 HV 0.01), thereby emphasizing the significant influence of intermetallic phases on the material's hardness characteristics. Further, enhanced specific compression strength was observed on a V–9Si–13B alloy within the temperature range of 600 °C to 1100 °C [1]. The results indicate that the compressive yield stress of the alloy V–9Si–13B is comparable to that of a Nibased superalloy (CMSX-4) at 1000 °C, and even superior at lower temperatures. Notably, the density of the V–9Si–13B alloy (ρ = 5.85 g/cm^3) is only 70 % of the CMSX-4 alloy (ρ = 8.7 g/cm^3) materials [1]. To increase the specific performance of V–Si–B alloys, titanium has been added to the V–based materials. The positive effect of titanium additions on density, mechanical properties and oxidation behavior was experimentally proved in Mo–Si–(B)–Ti alloys [6].

The conventional processing of V–based alloys using ingot metallurgy and subsequent machining is characterized by high energy and time requirements, primarily attributed to the disparate mechanical behavior exhibited by the ductile solid solution phase and the brittle silicides. Furthermore, a strong drawback stemming from the prevalent presence of a coarse-grained and non–uniform microstructure, a consequence of employing ingot processes was seen [7]. The implementation of an additive manufacturing (AM) approach as a single-step process for such materials may imply a significant breakthrough, enabling the fabrication of intricate bulk materials with geometries closely tailored to specific technical components, such as turbine blades [8]. Previous studies have demonstrated the successful utilization of additive manufacturing (AM) production pathways to achieve high-strength metallic components for conventional materials like steels or titanium alloys [9]. Experimental evidence indicates that additive manufacturing (AM) materials exhibit comparable tensile strength and Young's modulus compared to those observed in cast steel components, specifically SS 316 L parts [10].

Laser beams that are renowned for their high coherence and directionality find extensive application in the surface conditioning of various metal materials. The amount of available materials for laser beam melting (LBM) is still limited yet. Huber et al. already did research on the applicability of laser beam melting (LBM) as heat–treatment on tool steels [11]. In a review on laser beam melting (LBM) techniques the theoretical foundations of laser beam shaping techniques and their impact on melt pool dynamics, process stability, productivity, mechanical properties, microstructure, and surface roughness in laser-based powder bed fusion (L–PBF), as well as the various techniques and elements used to generate specific beam profiles was shown [12]. By appliying laser beam melting (LBM) with specific scanning parameters adapted to the particular metallic system, the melting and solidification lead to a tailored surface microstructure that may improve various material properties, e.g. wear and corrosion resistance. This study demonstrates for the first time the results of implementation of the laser beam melting on V-Ti-B alloys. The novelty of this work lies in assessing the feasibility of laser beam melting (LBM) in creating tailored microstructures that cause improvement of mechanical properties. The scientific contribution is significant as the laser beam melting (LBM) technique has rarely been applied on refractory metal–based systems. The intrinsic limitations of vanadium alloys and other refractory materials may, therefore, be overcome utilizing laser surface conditioning treatments [13].

2 | EXPERIMENTAL METHODS AND ALLOYS

The phase diagram V–Ti–B used to select alloys investigated in this study was calculated using a self–developed database. The data base was built using existing databases on the binary systems V–Ti, Ti–B and V–B and extended with the ternary databes V–Ti–B [14]. Four different alloys with titanium and boron concentrations ranging from 10 at.-% to 40 at.-% were chosen. The initial materials used in this study consisted of high-purity vanadium turnings (purity: 99.7 wt.-%), titanium granules (purity: 99.8 wt.-%), and boron granules (purity: 99.0 wt.-%). The as–cast state is reached after five cycles of arc melting and two cycles of levitation melting in an argon atmosphere. The loss of material in all samples was minimal in relation to their initial mass, i.e. less than 1.0 wt.-%. The chemical compositions of the alloys were determined using inductively coupled plasma–optical emission spectrometry (ICP-OES/iCap 7600). The measured compositions are in good agreement with the nominal chemical composition of the alloys, Table 1.

The surface of the fabricated specimen were remelted using a TruLaser Cell 3000 (Trumpf) 3D Lasermelting system in ambient atmosphere twice with two sets of parameters, Table 2. The selective laser melting (SLM) parameters are adapted from the publication by Schmelzer et al. [15]. To study the effect of the laser beam power on the microstructure of the alloys studied, two different values of the laser beam power were applied. The surface laser treatment was applied on four different alloys to determine its applicability to alloys with a varying boron and titanium content and to identify suitable parameters such as laser beam power.

Prior to metallographic characterization, the samples were embedded in a resin containing copper, followed by grinding with silicon carbide (SiC) abrasive paper up to a grit size of #4000. Subsequently, polishing was performed using a 0.05 µm silicon suspension (OPS). The microstructure was examined using the scanning electron microscopy (SEM) equipped within a focused ion beam (FIB) FEI NanoLab 600. The elemental compositions were analyzed using energy dispersive x-ray spectroscopy (EDS) equipped within a Zeiss Ultra 55 scanning electron microscopy (SEM). Further, the alloys were investigated by x–ray diffraction (XRD) PANalytical X'Pert Pro and analyzed by Profex to identify the formed phases.

TABLE 1 Nominal and chemical compositions of the V-Ti-B alloys in as-cast state.

	Experimental values of the chemical compostion in at.-%		
Alloy	**V**	**Ti**	**B**
V–28Ti–40B	31.38	26.56	42.06
V–38Ti–10B	52.91	38.75	8.34
V–40Ti–30B	27.94	37.88	34.17
V–40Ti–40B	18.94	37.71	43.35

TABLE 2 Selective laser melting parameters used for the laser remelting process.

Parameter	Symbol	Unit	Values remelt 1	Values remelt 2
Laser beam power	P_L	W	120	180
Laser beam diameter	D	mm	0.6	0.6
Scanning velocity	v_v	mm/s	6.67	6.67

The microhardness measurements were performed on an apparatus from Struers (Struers Duramin 1) with a range of HV 0.5 10 to HV 2 10 (Vickers hardness). The indent was done with a force of 1 kp (HV 1 10) for 10 seconds and subsequently evaluated in the scanning electron microscopy (SEM) to reach a higher accuracy. For better understanding, a schemativ setup is generated, Figure 1.

The investigated alloys were chosen regarding the calculated phase diagram, Figure 2. For the calculation of this diagram, a thermodynamical database was used [14]. The database was created by the CALPHAD method by iterative improving of the thermodynamic parameters. The set of parameters can be taken out of the publication [12]. The alloys, which were used for laser beam treatment are marked by green dots. The phase diagram is also used to compare the alloys regarding the forming phases after laser beam treatment and their phase equilibrium.

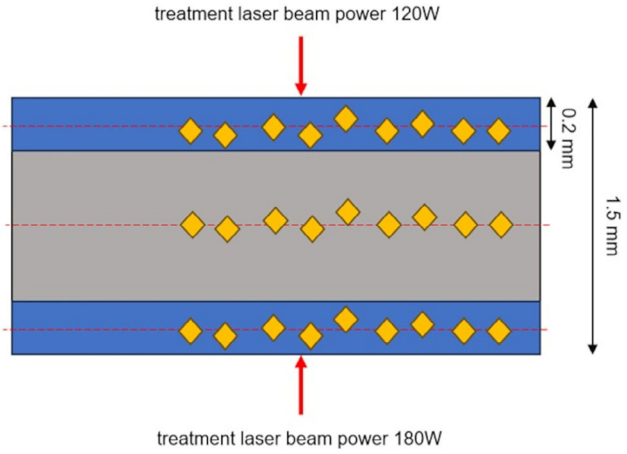

FIGURE 1 Schematic setup of the hardness testing.

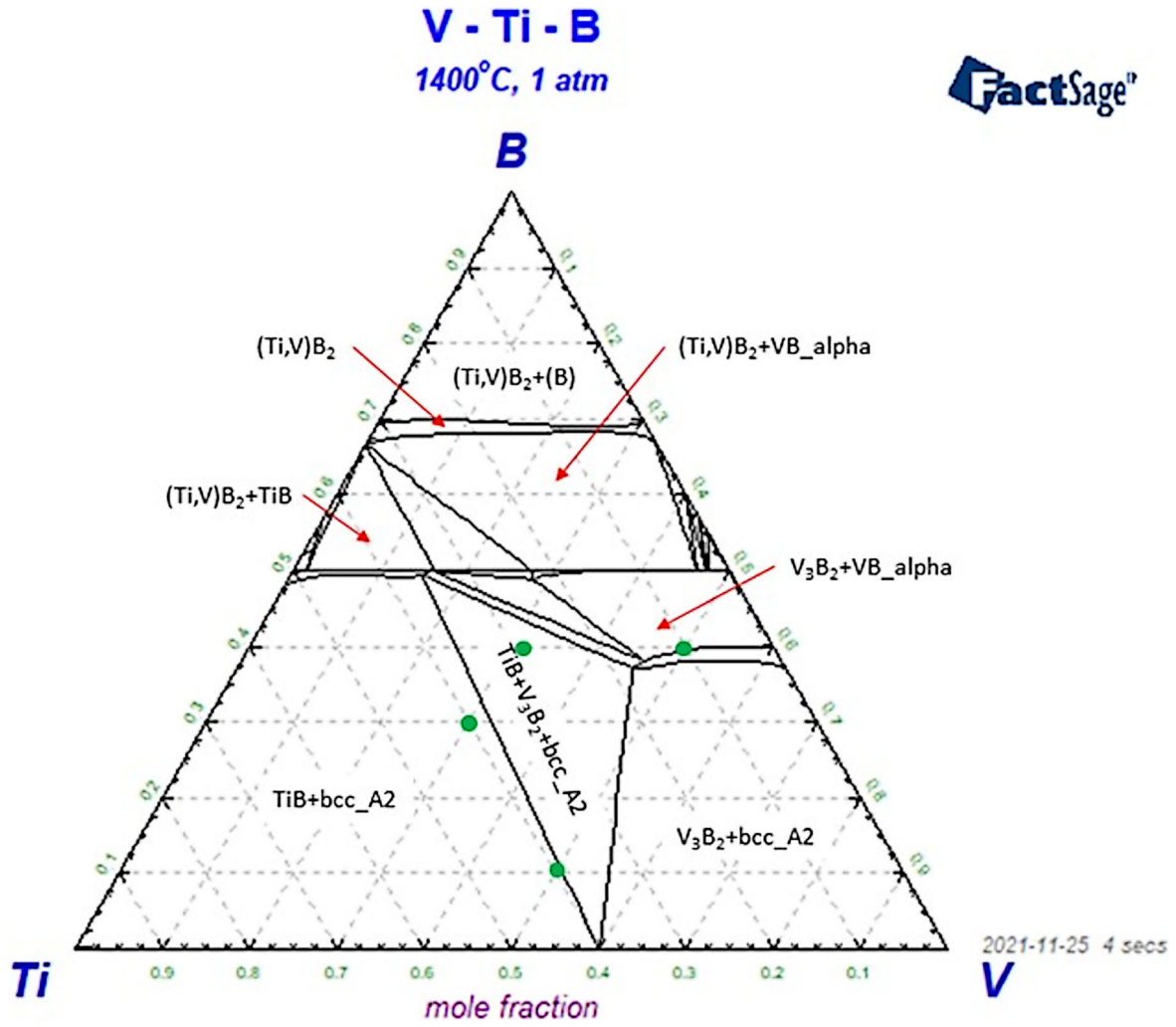

FIGURE 2 Calculated phase diagram using the database created in [12] which was used to choose the investigated alloys and calculated by using the software FactSage (alloys are marked by green dots).

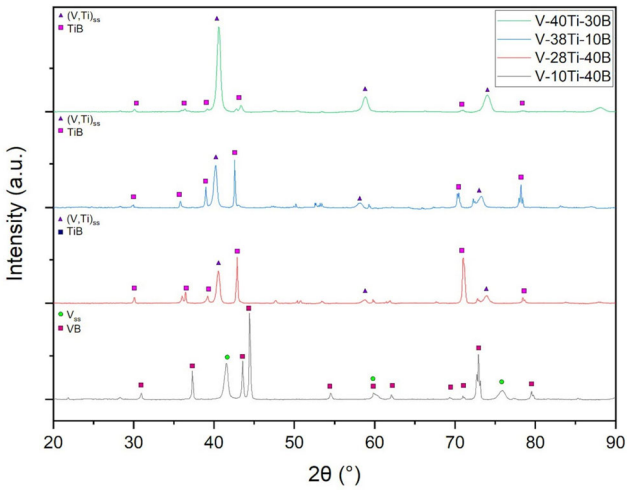

FIGURE 3 X-ray diffraction (XRD)-measurements of the alloys V-10Ti-40B, V-28Ti-40B, V-38Ti-10B, V–40Ti-30B in the as-cast state.

3 | RESULTS

To identify the phases present in the alloys in the as–cast condition, x–ray diffraction (XRD) analyses were conducted on alloys studied, Figure 3.

For comparison to the as-cast state, the laser beam treated surfaces were also analyzed by x-ray diffraction (XRD). Whereas the analysis of the as–cast specimens was performed on the cross-section, the measurements of the laser–treated surfaces were performed directly on the treated surfaces. The outcome of the x–ray diffraction (XRD) measurements on the laser-treated alloys reveal the present phases in the alloys, Figure 4a, b. Only the V–40Ti–30B alloy exhibits an equilibrium state following laser beam treatment at a power of 120 W. However, after laser treatment at 180 W, the alloy transitions to a non-equilibrium state, forming the Ti_3B_4 and TiB phases. In contrast, the V–38Ti–10B alloy does not undergo any

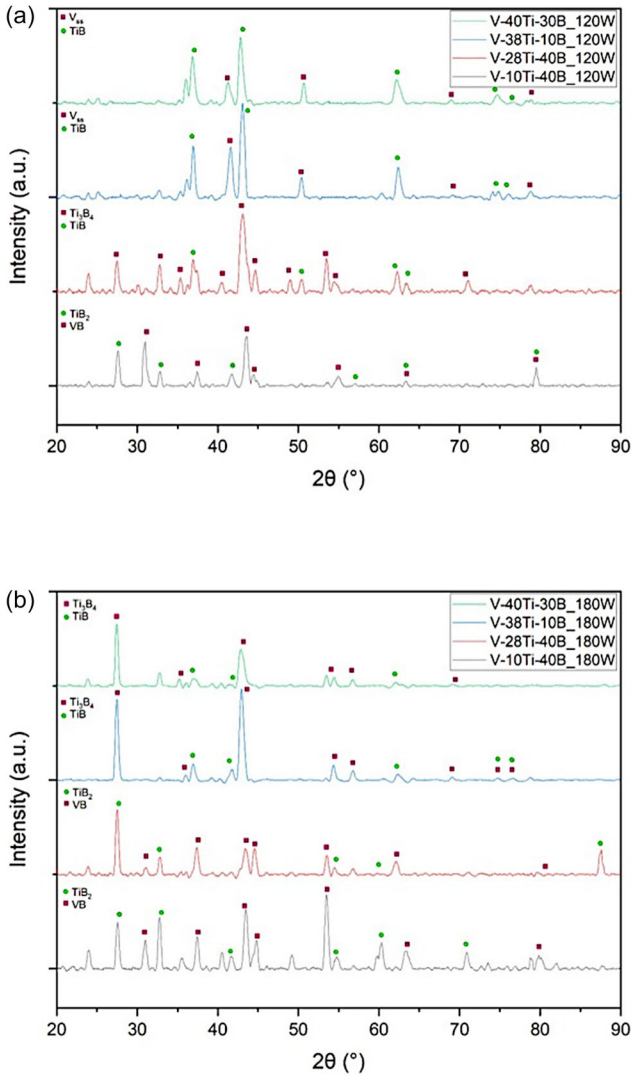

FIGURE 4 X-ray diffraction (XRD)-measurements of the alloys V-10Ti-40B, V-28Ti-40B, V-38Ti-10B, V–40Ti-30B after laser treatment with a laser power of (a) 120 W and (b) 180 W.

phase transformation after laser treatment at 120 W. Similar to the first alloy, the second alloy also forms Ti_3B_4 and TiB phases after laser treatment at 180 W. The third and fourth alloys exhibit the formation of Ti_3B_4 and TiB phases at 120 W, while laser treatment at 180 W leads to the formation of TiB_2 and VB phases. X–ray diffraction (XRD) analysis was conducted to examine the impact of laser irradiation and its influence on phase formation, as demonstrated for the first alloy, which exhibits distinct phase compositions after treatment at 120 W and 180 W.

3.1 | Alloy V–10Ti–40B

The alloy denoted as V-10Ti-40B exhibits the presence of a body-centered cubic V solid solution phase along with the VB phase in the as-cast state. The microstructural characteristics after the laser treatment were investigated via scanning electron microscopy (SEM) micrographs in BSE mode, Figure 5. To evaluate the effect of the laser beam on the properties of the alloy surface, the hardness measurements were performed (I) at a distance of ~ 150 μm from the surface, (II) at the geometric center of the 1.5 mm thick specimen. The analysis of the indents was carried out using the backscattered electrons (BSE) mode scanning electron microscopy (SEM) micrographs and ImageJ visualization. Additionally, the element concentrations of distinct phases in the core of the specimen were determined, Figure 6, Table 3. The influence of the laser treatment exhibits a change in the chemical constitution of the alloy. Regarding the x-ray diffraction (XRD) measurements in conjunction with the chemical constitution of the alloy, this may suggest that the ductile V_{ss} phase transforms into the TiB_2 phase on the surface, Figure 4a, b.

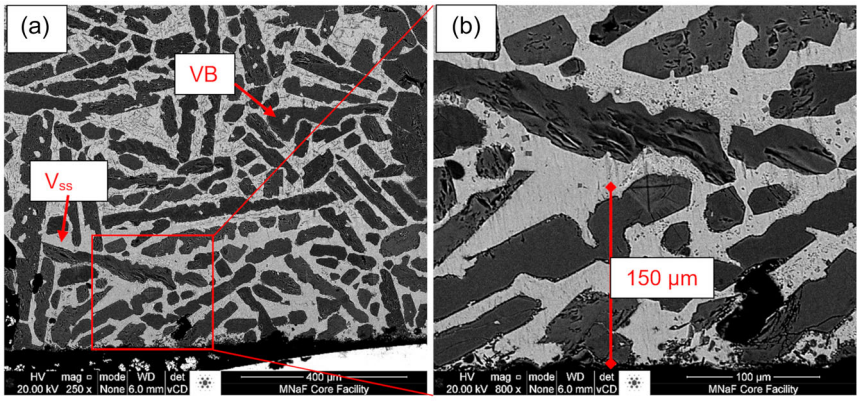

FIGURE 5 Scanning electron microscopy (SEM) micrographs in BSE mode of the alloy V-10Ti-40B surface treated with a power of 180 W showing the dark VB phase and the bright V_{ss} matrix (a) and a detailed image (b) to show the Vickers indent.

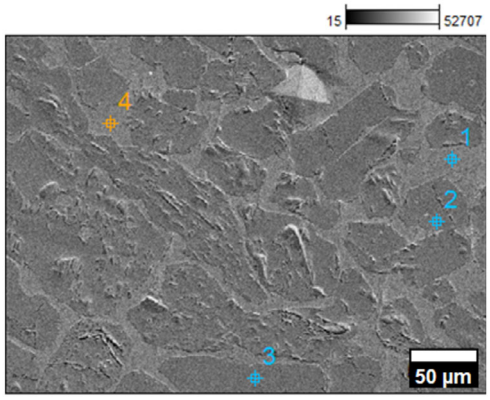

FIGURE 6 Scanning electron microscopy (SEM) micrograph of the laser treated V-10T-40B alloy with energy dispersive x-ray spectroscopy (EDS) measurement marks related to Table 3.

TABLE 3 Measured concentrations of elements (energy dispersive x-ray spectroscopy (EDS)) in phases recalculated with assumed stoichiometric B-contents of alloy V–10Ti–40B.

	B (at.-%)	Ti (at.-%)	V (at.-%)
Spot 1	-	21.13	78.87
Spot 2	(50.00)	6.12	43.88
Spot 3	(50.00)	5.99	44.01
Spot 4	-	13.92	76.08

The hardness assessment of the V–10Ti–40B specimen yielded an approximate mean value of 1050 HV 10 across the entire thickness of the sample. Both surface measurements exhibit an average hardness of 1100 HV 10, whereas the core of the specimen demonstrates a hardness of 1000 HV 10, Figure 7. This suggests that the chosen parameters for the laser 3D surface conditioning alter the alloy properties moderately. In terms of the median values extracted from the measurements, it is discernible that the laser surface conditioning conducted at 120 W yields a median hardness of approximately 750 HV 10 within the interquartile range (25 % - 75 %), whereas the 180 W conditioning manifests a median hardness of approximately 1200 HV 10. Conversely, the median hardness of the core measurements amounts to approximately 900 HV 10. These observations imply that the laser conditioning employing a power of 180 W may potentially exert a more pronounced influence compared to the lower power setting of 120 W.

3.2 | Alloy V–28Ti–40B

The second alloy with a composition of V-28Ti-40B demonstrates a two-phase microstructure encompassing the body-centered cubic $(V,Ti)_{ss}$ phase alongside the TiB phase. The microstructural peculiarities of this alloy show the $(V,Ti)_{ss}$ phase as matrix with TiB precipitates, Figure 8. The hardness measurements were conducted using the same methodology as for the preceding specimen, involving measurements at a distance of approximately 150 µm and measurements at the geometric center of the sample. The elemental concentrations of the distinct phases were measured by energy dispersive x-ray spectroscopy (EDS), Figure 9, Table 4:

The hardness assessments of the second alloy revealed an elevated hardness of the laser–modified surface as a consequence of the employed power of 120 W. The mean hardness registered approximately 2000 HV 10, while the surface modified at 180 W demonstrated an average

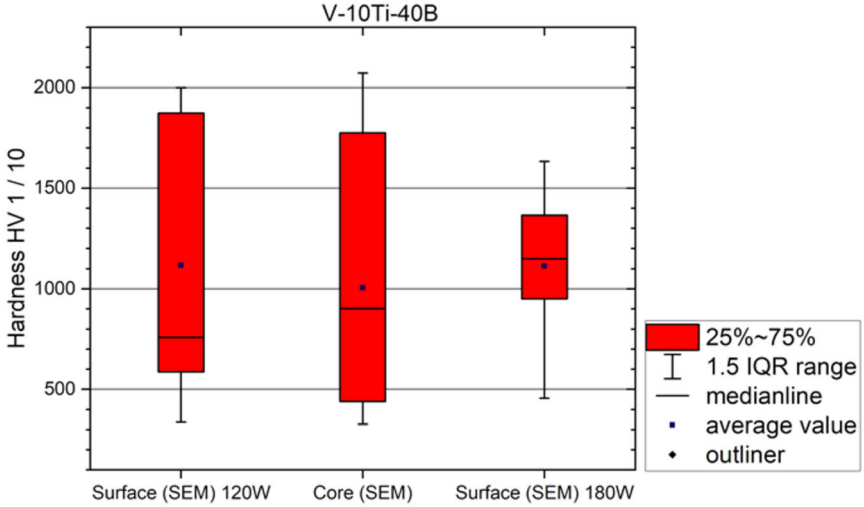

FIGURE 7 Results of the hardness measurements for the modified surfaces with a power of 120 W and 180 W and the core hardness values of alloy V-10Ti-40B.

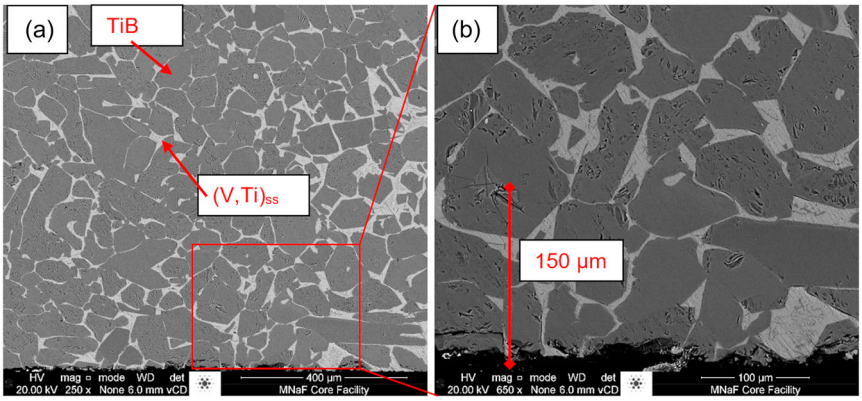

FIGURE 8 Scanning electron microscopy (SEM) micrographs in BSE mode of the alloy V-28Ti-40B surface treated with a power of 120 W showing the dark TiB phase and the bright $(V,Ti)_{ss}$ matrix (a) and a detailed image (b) to show the Vickers indent.

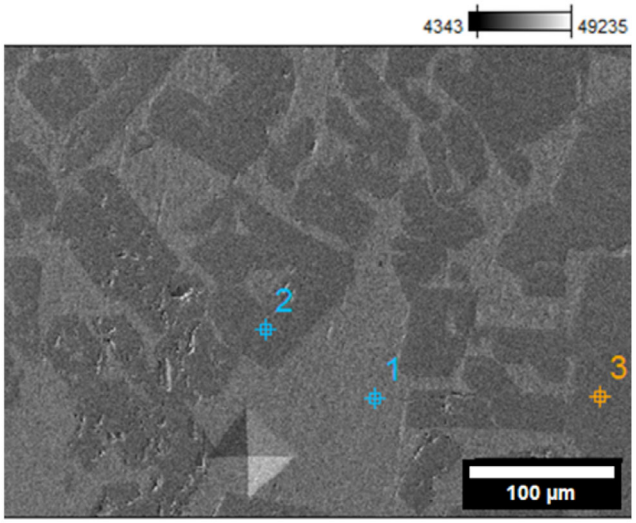

FIGURE 9 Scanning electron microscopy (SEM) micrograph of the laser treated V-28T-40B alloy with energy dispersive x-ray spectroscopy (EDS) measurement marks related to Table 4.

TABLE 4 Measured concentrations of elements (energy dispersive x-ray spectroscopy (EDS)) of phases recalculated with assumed stoichiometric B-contents of alloy V–28Ti–40B.

	B (at.-%)	Ti (at.-%)	V (at.-%)
Spot 1	-	75.38	24.62
Spot 2	(50.00)	44.06	5.94
Spot 3	(50.00)	44.06	5.94

hardness of approximately 1520 HV 10, Figure 10. The hardness of the specimen core yielded a value of around 1490 HV 10. Notably, the median hardness values within the interquartile ranges on the surface closely align with the computed averages. In the central region of the specimen, the median value slightly surpasses the calculated average, registering at approximately 1520 HV 10.

The above findings suggest a favorable alteration of the surface treatment with a 3D laser power of 120 W. A substantial difference of approximately 500 HV 10 between the surface and the core hardness was detected. Conversely, the conditioning employing a laser power of 180 W yields less pronounced effects with respect to hardness values. The chemical composition of the surfaces reveals Ti_3B_4 and TiB phases on the 120 W treated surface, whereas the opposite surface shows VB and TiB_2 phases.

3.3 | Alloy V–40Ti–30B

The V-40Ti-30B alloy exhibits a two-phase microstructure and is characterized by the presence of the body-centered cubic phase $(V,Ti)_{ss}$ and the TiB phase, Figure 11. The alloy V–40Ti–30B underwent the identical analysis as the two previous alloys, with indentation performed at a distance of 150 µm from the surface and at the geometric center of the specimen to identify the original hardness of the alloy. The constitutions of alloy phases and locations of measurement were identified and located equally to the previous specimen, Figure 12, Table 5.

The hardness evaluation exhibits an average value of approximately 800 HV 10 across the entire thickness of the specimen. Moreover, the median value within the interquartile range for the entire specimen surface shows hardness values between 700 HV 10 and 800 HV 10. This observation suggests that there is minimal impact of the laser surface treatment on the alloy microstructure, Figure 13. The chemical analysis of the surfaces reveals the same phase formations as in the previous alloy. The surface treated with a lower energy forms a microstructure consisting of V solid solution and TiB, whereas the opposite surface reveals formation of Ti_3B_4 and TiB.

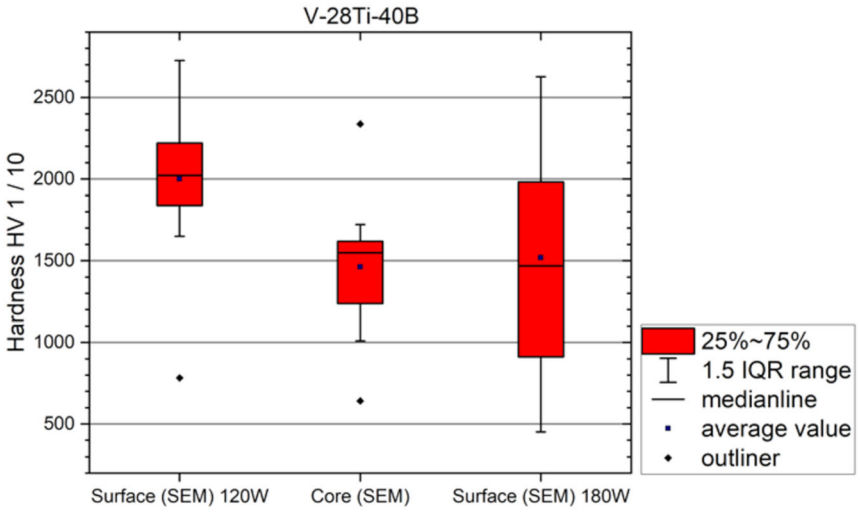

FIGURE 10 Results of the hardness measurements for the modified surfaces with a power of 120 W and 180 W and the core hardness values of alloy V-28Ti-40B.

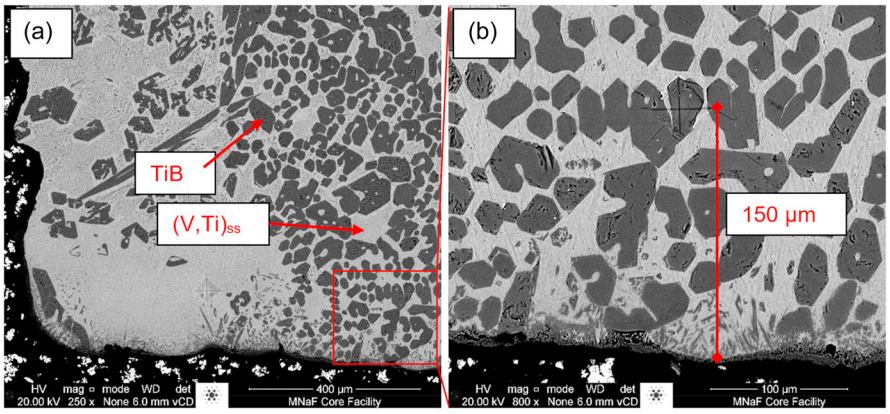

FIGURE 11 Scanning electron microscopy (SEM) micrographs in BSE mode of the alloy V-40Ti-30B surface treated with a power of 180 W showing the dark TiB phase and the bright $(V,Ti)_{ss}$ matrix (a) and a detailed image (b) to show the Vickers indent.

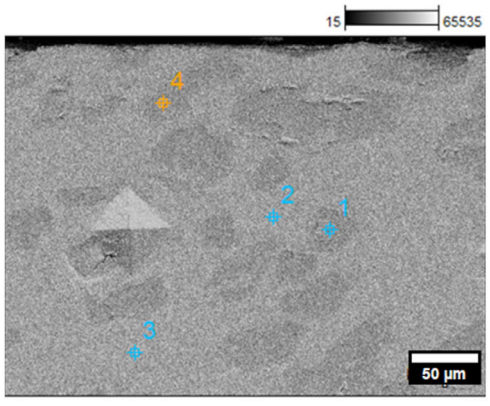

FIGURE 12 Scanning electron microscopy (SEM) micrograph of the laser treated V-40Ti-30B alloy with energy dispersive x-ray spectroscopy (EDS) measurement marks related to Table 5.

TABLE 5 Measured concentration of elements (energy dispersive x-ray spectroscopy (EDS)) of phases recalculated with assumed stoichiometric B-contents of alloy V–40Ti–30B.

	B (at.-%)	*Ti (at.-%)*	*V (at.-%)*
Spot 1	(50.00)	29.94	20.06
Spot 2	-	77.41	22.59
Spot 3	-	83.61	16.39
Spot 4	(50.00)	29.41	20.59

3.4 | Alloy V–38Ti–10B

The alloy V-38Ti-10B exhibits a two-phase microstructure consisting of the body-centered cubic phase $(V,Ti)_{ss}$ and the TiB phase as the specimen before, Figure 14. The surface layer shows cracks with a length of approx. 120 µm

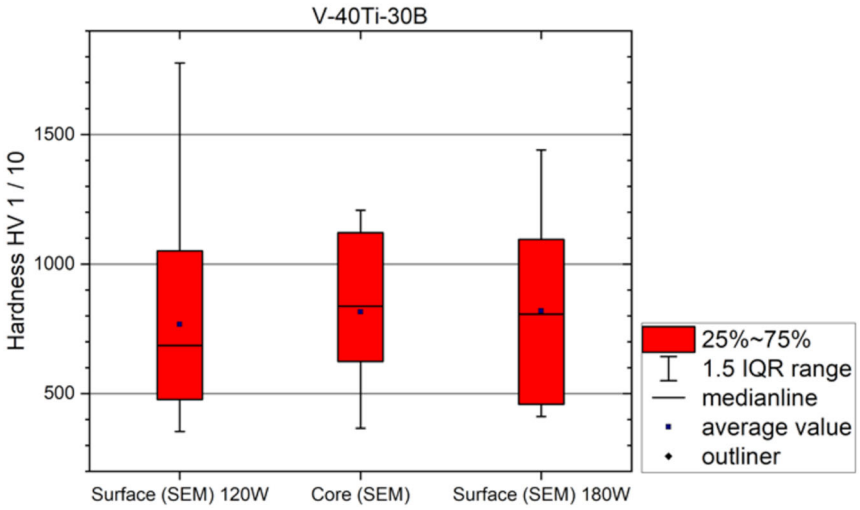

FIGURE 13 Results of the hardness measurements for the modified surfaces with a power of 120 W and 180 W and the core hardness values of alloy V-40Ti-30B.

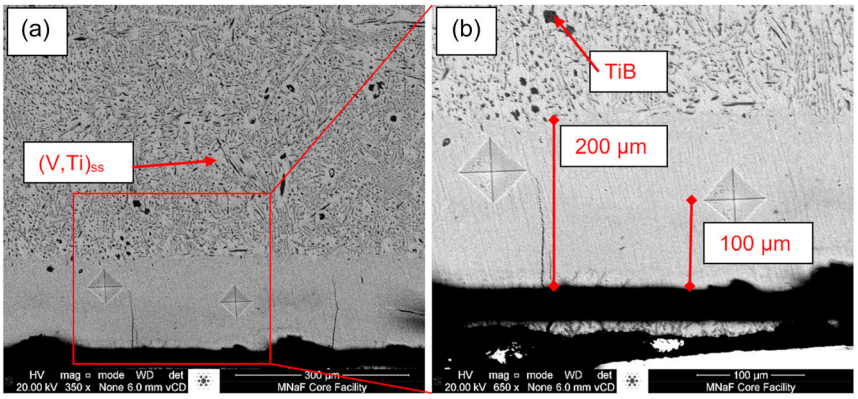

FIGURE 14 Scanning electron microscopy (SEM) micrographs in BSE mode of the alloy V-38Ti-10B surface treated with a power of 120 W showing the dark TiB phase and the bright $(V,Ti)_{ss}$ matrix (a) and a detailed image (b) to show the Vickers indent.

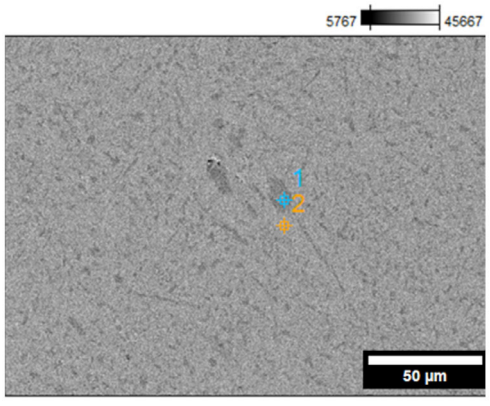

FIGURE 15 Scanning electron microscopy (SEM) micrograph of the laser treated V-38T-10B alloy with energy dispersive x-ray spectroscopy (EDS) measurement marks related to Table 6.

to 130 µm, Figure 14. This observation may indicate increased surface brittleness attributable to an enhanced hardness induced by the laser treatment of the specimen. An alternative explanation could be that the laser treatment induces thermal stress on the surface, leading to the formation of stress cracks.

In contrast to the preceding hardness measurements, the indents in this alloy were conducted at a depth of 100 µm. This deviation from the earlier procedure is justified by the presence of a surface layer with a thickness of approximately 200 µm that formed as a consequence of laser beam treatment. Taking the fine lamellar eutectic structure into account, two energy dispersive x-ray spectroscopy (EDS) spot measurements were performed and the elemental compositions were identified, Figure 15, Table 6.

The hardness measurements for the V-38Ti-10B alloy yielded results akin to the previous alloy V–40Ti–30B.

TABLE 6 Measured concentration of elements (energy dispersive x-ray spectroscopy (EDS)) of phases recalculated with assumed stoichiometric B-contents.

	B (at.%)	*Ti (at.%)*	*V (at.%)*
Spot 1	(50.00)	26.68	23.32
Spot 2	-	63.95	36.05

The surface treated with the lower laser power (120 W) exhibited an enhanced hardness when compared to both the core and the surface subjected to laser treatment at 180 W. The calculated mean and median values within the 25 % to 75 % range for the modified surface hardness are approximately 500 HV 10. On the contrary, the mean hardness for the opposing surface (treated with 180 W) revealed a value of 390 HV 10 with the median of the interquartile range measuring around 360 HV 10. The core displayed a mean hardness and median value of 340 HV 10. Although a lower hardness increase as observed for the V–28Ti–40B alloy was detected, there is still a hardness increase of approximately 110 HV 10 due to the laser beam treatment, Figure 16.

The phase analysis of the surfaces of the alloy V–38Ti–10B reveals the phases V_{ss} and TiB on the 120 W treated surface and Ti_3B_4 and TiB on the 180 W treated side. The chemical impact on the 120 W surface seems to be lower as no phase transformation was observed, whereas Ti_3B_4 phase was found on the 180 W treated surface.

As mentioned above, the alloy V–38Ti–10B exhibited a surface layer with a thickness of approximately 200 µm, Figure 17. The surface subjected to the laser beam treatment exhibits a layer characterized by a microstructure that is distinctively different from the microstructure inherent to the core of the specimen. The transition region between the layer arising from the laser beam treatment and the core shows a microstructural delineation, Figure 17c, d. The surface layer seems to form three different microstructures. The surface exhibits a morphology akin to a dendritic microstructure, Figure 17 b. In contrast, the transition zone between the layer and the core displays a lamellar microstructure with an embedded secondary phase, Figure 17 d.

The surface layer of the V–38Ti–10B alloy subjected to the 180 W treatment regime shows a discernible contrast in the transition zone when compared to the surface layer treated at 120 W, Figure 18. The thickness of the surface layer after the 180 W treatment is approximately quantified at 300 µm. Comparative analysis with the surface treated at 120 W unveils localized concentrations of dendritic structures indicative of boride phases, Figure 18c, d.

4 | DISCUSSION

In light of the findings of the four analyzed alloys, the supposition that surface conditioning is attainable through laser treatment is substantiated. While the V–40Ti–30B and V–10Ti–40B alloys exhibit moderate enhancement in hardness when subjected to both 120 W and 180 W laser beam powers, the V–28Ti–40B and V–38Ti–10B alloys show appreciable hardness increase. The hardness profile of the V–40Ti–30B alloy remains relatively constant across its entirety, yielding an approximate value of 800 HV 10. Similarly, the V–10Ti–40B alloy maintains an almost uniform hardness, averaging around 1000 HV 10. This suggests that the impact of laser–induced surface

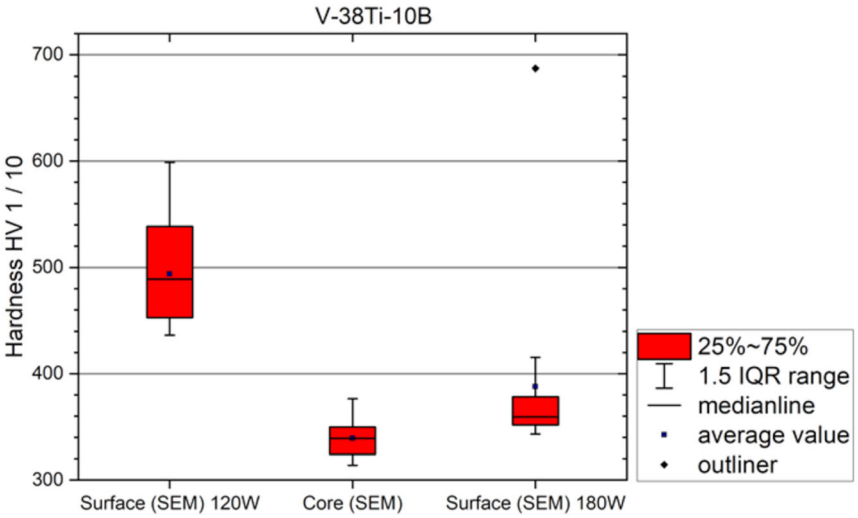

FIGURE 16 Results of the hardness measurements for the modified surfaces with a power of 120 W and 180 W and the core hardness values of alloy V-38Ti-10B.

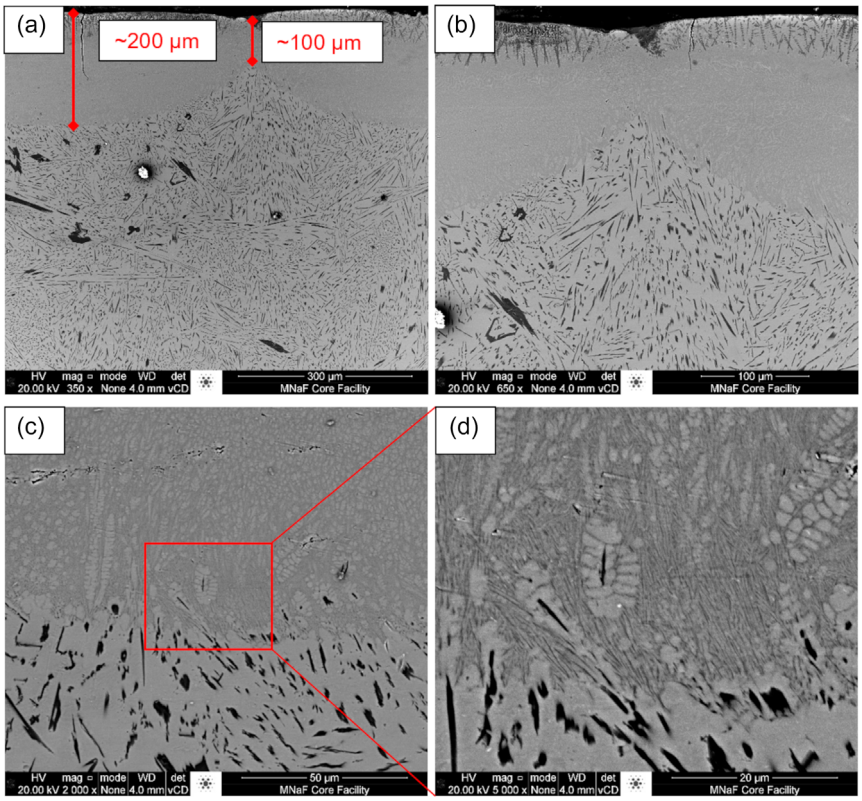

FIGURE 17 Scanning electron microscopy (SEM) micrograph in BSE mode of the cross-section of the V-38Ti-10B alloy treated with a power of 120 W revealing the eutectic core structure (a), a detailed magnification of the formed surface layer (b), transition zone of the layer into the core microstructure (c) and a detailed magnification of the marked area (red square) (d).

treatment, employing the parameters applied in this work, is relatively subdued for these alloys, Table 2. This could be attributed to the laser's velocity during the remelting process. A slower velocity may enhance the influence of the heat-affected zone on mechanical properties.

The V–28Ti–40B alloy demonstrates an even more substantial impact from surface conditioning, showcasing an average hardness increase of 500 HV 10 (33 % increase in hardness regarding core average) with the 120 W treatment, while the 180 W treatment shows a comparatively limited effect on alloy hardness (5 % increase in hardness regarding core agerage). The origin of this significant difference is still unclear. In contrast, the V–38Ti–10B alloy exhibits escalating hardness on both treated surfaces, with the 120 W treatment resulting in a more pronounced effect compared to the 180 W treatment. Notably, both sides display a discernible increase in hardness, amounting to 180 HV 10 (56 % increase in hardness regarding core agerage) and 70 HV 10 (22 % increase in hardness regarding core agerage) for 120 W and 180 W treatments, respectively. Upon examination of the resultant surface layer the site treated at 120 W exhibits a more uniform layer relative to that of the 180 W treated surface of the specimen. The hardness disparity is postulated to originate from the ensuing microstructural differences. The 120 W treated surface is characterized by a fine lamellar microstructure with an embedded second phase, whereas the surface subjected to 180 W treatment displays a pronounced dendritic morphology. Additionally, clusters of dendritic precipitations are discernible within the surface layer. Such microstructural features may contribute to the comparatively modest enhancement in hardness associated with the surface layer treated at the higher energy level. Both surfaces show cracks, which could be caused by the laser treatment and the resulting heat energy that is introduced to the specimen surface. This may result in thermal stress on the surface and facilitate crack initiation. The cracks are also an indication of higher surface brittleness compared to the other specimen.

Among all specimens subjected to analysis, the alloy V–38Ti–10B uniquely exhibits a surface layer sensible to the laser treatment. It is proposed that this phenomenon is due to the specimen's diminished boron content. In contrast to the other specimens, this compositional variance results in a reduced presence of borides, which are recognized for their high thermodynamic and thermal stability. While other alloys possess a high amount of coarse globular boron precipitates, the distinct feature of the alloy

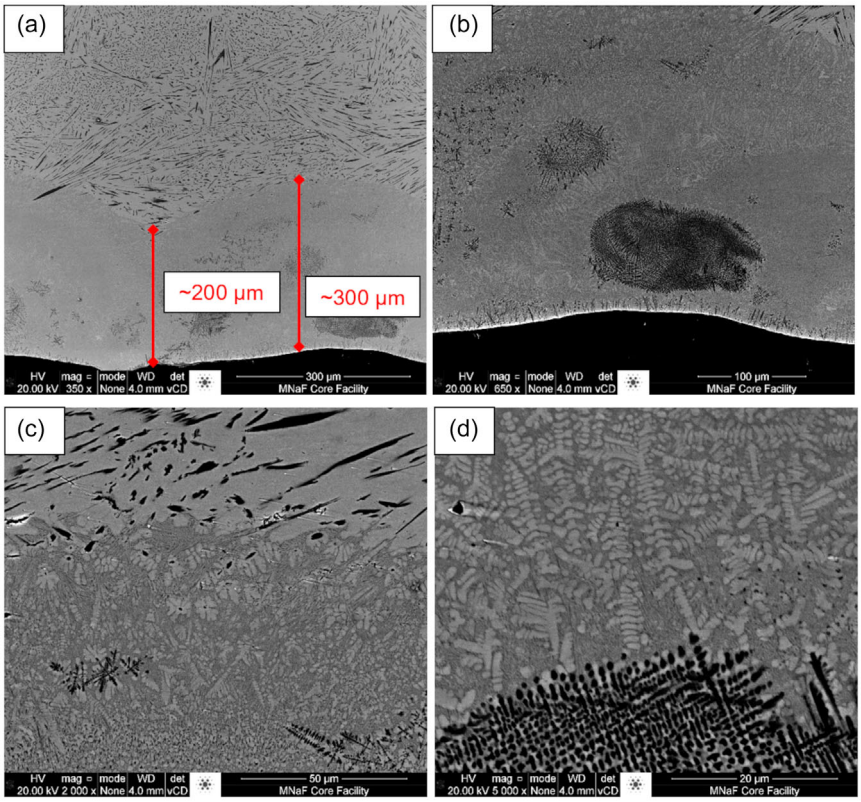

FIGURE 18 Scanning electron microscopy (SEM) micrograph in BSE mode of the cross-section of the V-38Ti-10B alloy treated with a power of 180 W revealing the eutectic core structure (a), a detailed magnification of the formed surface layer (b), transition zone of the layer into the core microstructure (c) and a detailed magnification of the cluster of dendritic boride phases (d).

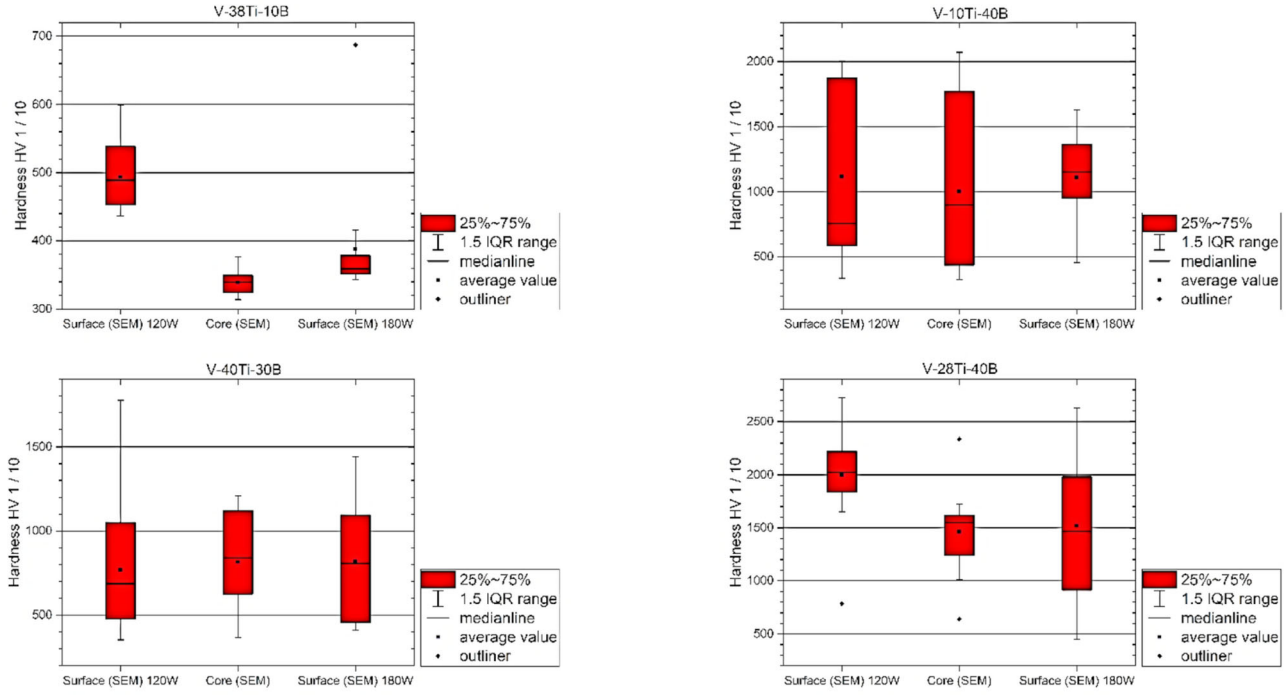

FIGURE 19 Comparison of all hardness measurement results for the alloys V–38Ti–10B, V–10Ti–40B, V–40Ti–30B and V–28Ti–40B.

V–38Ti–10B is clearly its very fine microstructure which is apparently vulnerable to laser treatment.

When comparing the varying titanium and boron contents in the investigated alloys, it appears that an increasing boron concentration reduces the susceptibility of the alloy to laser treatment. In contrast, the titanium content does not exhibit a significant influence on the alloy's response to laser processing. However, a higher titanium content in combination with a lower boron concentration promotes the formation of a lamellar microstructure, whereas an increased boron content favours the development of a globular microstructure. Nevertheless, there appears to be an optimal concentration range, as the alloy V–28Ti–40B also exhibits favourable susceptibility to laser treatment. The responses to the laser treatments are underlined and confirmed by hardness measurements throughout all alloys and compared to each other, Figure 19.

These results underscore the feasibility of surface conditioning through 3D laser treatment on alloys especially with fine microstructures. However, it is imperative to delve further into delineating the parameter effects within the laser setup. Additionally, an investigation into the alloy's liquidus projection could yield insights into chemical processes and phase formation temperatures, thus contributing to a comprehensive understanding of the resulting phase constitution and ensuing of the system.

5 | SUMMARY

In this study, the surfaces of four V-based alloys, V–38Ti–10B, V–40Ti–30B, V–10Ti–40B, and V–28Ti–40B, underwent laser surface treatment with varying power levels of 120 W and 180 W, while maintaining a constant scanning velocity. The primary objective was to discern the influence of laser power on the microstructure evolution and respective hardness. Subsequent analysis encompassed scanning electron microscopy (SEM) investigations, energy dispersive x-ray spectroscopy (EDS) and x-ray diffraction (XRD) measurements on the diverse alloys to ascertain their microstructural attributes and chemical compositions. Further, the hardness of each specimen was measured at an approximate depth of 150 μm from the surface, as well as in the core, situated at the geometric center of each specimen.

Microstructural analysis revealed two–phase microstructure in all the alloys (V_{ss}, TiB, Ti_3B_4, VB, TiB_2) in various combinations, Figures 3, 4. The alloy V–38Ti–10B demonstrates three different microstructures in the surface layer.

The experimental findings unveil an increase in surface hardness for the V–38Ti–10B and V–28Ti–40B alloys, while the V–40Ti–30B and V–10Ti–40B alloys exhibit negligible response to the treatment. The alloy V–38Ti–10B demonstrates the highest sensitivity to the laser beam treatment, presumably due to the very fine microstructure and the lower phase fraction of borides. For this alloy, the hardness augmentation ranges approximately from 180 HV 10 to 500 HV 10 after the 120 W, and 70 HV 10 after the 180 W laser beam treatment. Other alloys possess a high volume fraction of thermally stable coarse boride which clearly demonstrated a high degree of resistance to the laser beam.

To attain a more extensive understanding of phase formation and the associated chemical process temperatures, in-depth investigations into the liquidus projection of the system are imperative. Furthermore, a comprehensive parameter analysis of the laser energy and scanning velocity is essential to unravel their intricate influence on surface conditioning of these alloys and its interrelation with properties of the system.

ACKNOWLEDGEMENTS

The authors acknowledge the Deutsche Forschungsgemeinschaft (DFG/project nb. 410338871) for the financial support and the Micro- and Nanoanalytics Facility (MNaF) of the University of Siegen for the technical support and microscopy. The authors also acknowledge the help of Mr. Daniel Morez for preparing and supporting the remelting process. We also thank C. Thomas (PGI–5, FZ Jülich) for providing access to the arc–melter.

Open Access funding enabled and organized by Projekt DEAL.

ORCID

M. Carrion Saldaña https://orcid.org/0000-0003-0376-6979

REFERENCES

1. M. Krüger, *Scr. Mater.* **2016**, *121*, 75.
2. S. J. Zinkle, H. Matsui, D. L. Smith, A.F. Rowcliffe, E. van Osch, K. Abe, V. A. Kazakov, *J. Nuc. Mater.* **1998**, *258–263*, 205.
3. K. Natesan, M. Uz, *Fusion Eng. Des.* **2000**, *51–52*, 145.
4. J. Williams, M. Akinc, *Intermetallics* **1998**, *6* (4), 269.
5. H. Nowotny, E. Dimakopoulou, H. Kudielka, *Monatsh. Chem.* **1957**, *88* (2), 180.
6. M. A. Azim, S. Burk, B. Gorr, H.-J. Christ, D. Schliephake, M. Heilmaier, R. Bornemann, P. H. Bolívar, *Oxid Met* **2013**, *80*, 231.
7. D. A. P. Reis, C. A. Nunes, A. Capri Neto, *RBAV* **2007**, *26*, (2), 79.
8. M. Wang, R. Li, T. Yuan, C. Chen, M. Zhang, Q. Weng, J. Yuan, *Int J Refract Met H* **2018**, *70*, 9.
9. T. Mukherjee, J. S. Zuback, A. De, T. DebRoy, *Nat. Publ. Gr.* **2016**, *6*, 1.

10. B. Zhang, L. Dembinski, C. Coddet, *Mater. Sci. Eng. A* **2013**, *584*, 21.
11. F. Huber, C. Bischof, O. Hentschel, J. Heberle, J. Zettl, K. Y. Nagulin, M. Schmidt, *Mater. Sci. Eng. A* **2019**, *742*, 109.
12. A. R. Bakhtari, H. K. Sezer, O. E. Canyurt, O. Eren, M. Shah, S. Marimuthu, *Adv Eng Mater* **2024**, *26*, 14.
13. Y. S. Tian, C. Z. Chen, S. T. Li, Q. H. Huo, *Appl. Sur. Sci.* **2005**, *242* (1-2), 177.
14. M. Yazlak, H.-J. Christ, W. Yang, G. Hasemann, M. Krüger, B. Gorr, *CALPHAD* **2022**, *79*, 102477.
15. J. Schmelzer, S.-K. Rittinghaus, K. Gruber, P. Veit, A. Weisheit, M. Krüger, *Addit. Manuf.* **2020**, *34*, 101208.

How to cite this article: M. Carrion Saldaña, W. Yang, G. Hasemann, H.-J. Christ, R. Schwaiger, M. Krüger, B. Gorr, A. von Hehl. *Materialwiss. Werkstofftech*. **2026**; *0*, 1-14, https://doi.org/10.1002/mawe.70124